

## Interplay between fluid circulation and Alpine metamorphism in the Monte Rosa whiteschist from white mica and quartz in situ oxygen isotope analysis by SIMS

CINDY LUISIER<sup>1,2,\*</sup>, LUKAS P. BAUMGARTNER<sup>1,†</sup>, ANNE-SOPHIE BOUVIER<sup>1,‡</sup>, AND BENITA PUTLITZ<sup>1</sup>

<sup>1</sup>Institute of Earth Sciences, University of Lausanne, 1015 Lausanne, Switzerland

<sup>2</sup>University of Rennes, CNRS, Géosciences Rennes UMR 6118, Rennes, France

### ABSTRACT

In situ oxygen isotope compositions of white mica and quartz have been used to characterize the interplay of metamorphism and fluid events between a metasomatic whiteschist and its granite protolith in the Monte Rosa nappe, Western Alps. New natural muscovite and phengite reference materials were calibrated for in situ Secondary Ion Mass Spectrometry (SIMS) oxygen isotope measurement. White mica and quartz oxygen isotope compositions were measured in situ in one whiteschist and two metagranites. Based on microtextural observation, phengite composition of white mica, and phase petrology modeling, it is possible to identify two events of fluid infiltration and one event of fluid expulsion, all of which were responsible for forming this unique whiteschist occurrence and for tracing its metamorphic evolution from late Permian intrusion to Alpine subduction and finally to the present day, exhumed whiteschist.

Metagranite samples contain three generations of white mica: igneous, high-*P* metamorphic, and late Alpine, retrograde compositions. In the whiteschist samples, we distinguish two distinct Alpine white mica generations: (1) prograde to peak generation and (2) retrograde generation.

The  $\delta^{18}\text{O}_{\text{VSMOW}}$  values of white mica and quartz from a whiteschist of 5.3 to 7.3‰ and 9.1 to 10.6‰ are significantly lower than in the metagranites, with 9.1 to 10.8‰ and 13.2 to 14.6‰, respectively. This indicates a complete recrystallization of the whiteschist protolith during intense fluid-rock interaction. Subsequent Alpine metamorphism transformed the protolith into the whiteschist. The isotopic composition of the whiteschist, fine-grained, retrograde white mica (5.3 to 6‰) is lower than that of the high-pressure phengite (6.2 and 7.5‰). The low  $\delta^{18}\text{O}$  values could be explained by infiltration of external fluids with  $\delta^{18}\text{O}$  values of 2 to 6‰. Such fluids would carry the isotopic signature of the serpentinites of the Piemonte-Liguria Ocean by either equilibration of fluids with or dehydration of serpentinites. Another, more simple explanation would be the infiltration of very small quantities of fluids leading to the breakdown of chloritoid. Local inheritance of the oxygen composition would then hide the origin of the fluids.

Isotope exchange temperatures calculated from high-*P* phengite-quartz pairs in whiteschist give an average temperature of  $440 \pm 50$  °C. These are lower than the best *T*-estimates from phase petrology of 570 °C, at 2.2 GPa. Igneous muscovite-quartz pairs in the metagranite yield  $400 \pm 40$  °C. Only one high-*P* phengite-quartz pair was analyzed, resulting in  $350 \pm 40$  °C. Greenschist facies, low silica phengites give an average temperature of  $310 \pm 10$  °C. Propagation of analytical uncertainty suggests large errors of 60 to 120 °C, due to the relatively small *T*-dependence of the quartz-white mica fractionation factor for oxygen isotopes.

**Keywords:** White mica reference material, SIMS, oxygen isotopes, Monte Rosa, whiteschist, fluid-rock interaction; Isotopes, Minerals, and Petrology: Honoring John Valley

### INTRODUCTION

White mica is stable under a wide range of pressure (*P*) and temperature (*T*) conditions (Bailey 1984). It participates in many important dehydration and melting reactions in regional and contact metamorphic environments (e.g., Gardien et al. 2000; Pattison and Harte 1991; Skora and Blundy 2010; Spear 1995) and is a tracer of fluid flow in hydrothermal systems (e.g., Bulle

et al. 2020). The growing understanding of white mica chemical and mechanical behaviors during orogenic processes allows a characterization of the conditions under which they crystallize and deform. Notably, the phengite solid-solution series has attracted much interest in the field of geothermobarometry, since individual substitutions are controlled by pressure and temperature conditions in buffered systems (Spear 1995). As an example, the Tschermak substitution of  $(\text{Mg,Fe})+\text{Si} \leftrightarrow 2\text{Al}$  is known to be promoted by an increase in pressure, which led to the initial experimental determination of the silica in phengite barometer by Massonne and Schreyer (1987). Oxygen isotope thermometry using quartz-muscovite or quartz-phengite (e.g., Eslinger et al.

\* E-mail: cindy.luisier@gmail.com. Special collection papers can be found online at <http://www.minsocam.org/MSA/AmMin/special-collections.html>.

† Orcid 0000-0003-2304-1772

‡ Orcid 0000-0002-5202-603X

1979; Zheng 1993) has also facilitated the temperature estimation, as they are present in association in most rock types. Other applications of oxygen isotopes in white mica in the domain of fluid-rock interactions include hydrothermal fluid characterization (Bulle et al. 2020).

Oxygen isotope analyses by laser fluorination techniques are precise ( $\pm 0.1\%$   $1\sigma$ ) but require time-intensive, careful mineral separation, a task made difficult especially in polymetamorphic rocks, where several generations of the same mineral can coexist. In addition, imperfect mineral species separations, as caused by, for example, the presence of various inclusions, can introduce a bias in the isotopic signal of any given mineral, rendering thermometry and interpretation of oxygen isotope signal spurious. In situ measurements of stable isotopes by secondary ion mass spectrometry (SIMS) have improved our capability of observing the spatial relationship between the analyzed phases and promote a better in-depth understanding of the data obtained. To take advantage of this technique, it is paramount to have matrix matched reference materials (e.g., Marger et al. 2019; Siron et al. 2017; Valley and Kita 2009). The minimization of surface topography during sample preparation as well as the use of isotopically homogeneous reference materials has increased the analytical precision over the years, allowing a wide range of geological materials to be studied (e.g., Kita et al. 2011; Valley and Kita 2009). To our knowledge, white mica reference materials have been missing in the petrology toolbox so far. Therefore, we describe and characterize four white mica standards, which cover a wide range of celadonite content, designed to analyze phengitic muscovites.

The white mica standards are applied to the study of whiteschists from the Monte Rosa nappe (Western European Alps), which have been the focus of numerous studies (Chopin and Monié 1984; Le Bayon et al. 2006; Luisier et al. 2021, 2019; Marger et al. 2019). Whiteschists have been defined by Schreyer (1973) as high-pressure, Mg- and Al-rich rocks, in which the mineral association talc-kyanite or talc-chloritoid is commonly found

(Chopin 1985; Schreyer 1974). The Monte Rosa whiteschist shows the high-pressure paragenesis of chloritoid, talc, phengite, and quartz, with locally rare kyanite, garnet, and carbonate. The origin of whiteschists in the Alps is still debated (Ferrando 2012). While alteration by ultramafic derived fluids during prograde to peak Alpine conditions were proposed for the Dora-Maira whiteschist (see Ferrando 2012 for a review), the genesis of the Monte Rosa whiteschists has been explained by metasomatic alteration of the granite by late magmatic-hydrothermal fluids (Luisier et al. 2021; Pawlig and Baumgartner 2001). Luisier et al. (2021) have demonstrated that the chemistry of the whiteschist was acquired before the onset of Alpine metamorphism. The mineral assemblages now observable in the whiteschist and metagranite result from a combination of Alpine metamorphism and the deformation relative to the nappe emplacement and exhumation.

In this study, we use white mica and quartz oxygen isotope compositions in metagranite and associated metasomatic whiteschist from the Monte Rosa nappe, in the Western Alps (Fig. 1a), to track the interplay between fluid fluxes and metamorphism. The aim is to combine white mica and quartz isotopic compositions with microstructural observations and major element compositions to identify the potential extent and nature of fluid fluxes between a metasomatic whiteschist and its metagranite protolith during the Alpine history of the Monte Rosa nappe.

## GEOLOGICAL SETTING

The Monte Rosa nappe is part of the Penninic domain of the Western Alps (Fig. 1a). It belongs to the Internal Crystalline Massifs, together with the Gran Paradiso and Dora Maira. From a paleogeographic point of view, it corresponds to the southernmost tip of the Briançonnais microcontinent and hence represents the deepest subducted part of the European continental crust involved in the Alpine orogeny (Steck et al. 2015). The nappe consists of a pre-Alpine polymetamorphic paragneiss unit, in which granodioritic to granitic bodies intruded during

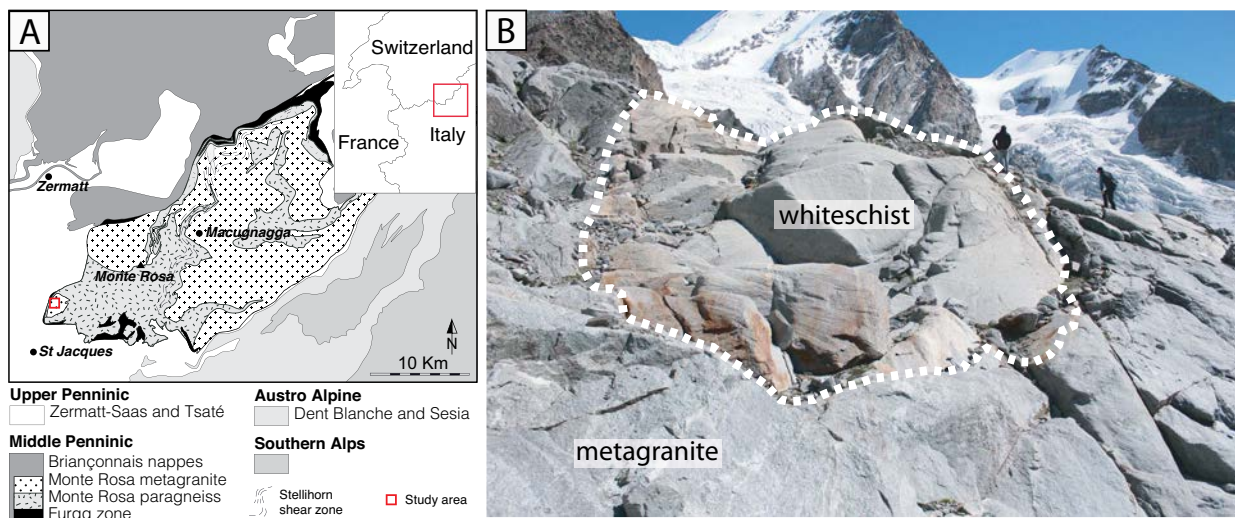


**FIGURE 1.** (a) Tectonic map showing the geology of the Monte Rosa nappe within the Western Alpine framework (modified after Steck et al. 2015). (b) Picture of the whiteschist outcrop. The transition zone with the surrounding metagranite is marked by the white dashed line. (Color online.)

the Permian (Beath 1952; Dal Piaz 2001), dated by SHRIMP U-Pb on zircon at  $269 \pm 4$  Ma (Pawlig 2001). The granite locally grades into 10 to 50 meter bodies of whiteschist (Fig. 1b). The whiteschists are metasomatic alteration products of the Monte Rosa granite. The metasomatism occurred pre-Alpine, likely during late hydrothermal alteration of the cooling granite intrusion (Luisier et al. 2021; Pawlig and Baumgartner 2001). Subsequently, the mineralogy was produced during Alpine high-pressure metamorphism (Luisier et al. 2019; Marger et al. 2019). The peak high-pressure Alpine metamorphism has been dated at  $42.6 \pm 0.6$  Ma (Lapen et al. 2006), by U/Pb geochronology on rutile in an eclogite of the Monte Rosa nappe. The *P-T* conditions for the peak metamorphism are estimated based on whiteschist phase petrology between 1.6 to 2.7 GPa for a temperature range of 490 to 575 °C (Chopin and Monié 1984; Le Bayon et al. 2006; Luisier et al. 2019). An age range between 42 to 39 Ma has been found for the post-peak retrogression to upper greenschist facies (Skora et al. 2015), based on Rb/Sr dating on phengite.

The study area is located to the North of the Mezzalama refuge, in the upper Ayas Valley, in Italy. Here, the Alpine metamorphism is heterogeneously recorded through the nappe and tightly related to the deformation intensity. Large volumes of rocks were very little deformed during the nappe formation and exhumation. Deformation is concentrated in high-strain areas, such as thin shear zones, as observed, for example, in the metagranite around the studied whiteschist body (Vaughan-Hammon et al. 2021). Here, we focus on the whiteschist body described in detail by Luisier et al. (2021), which is ellipsoidal. It is a cross-section through a whiteschist pipe (Luisier et al. 2021, 2019). The central part of the whiteschist body consists of an Alpine peak pressure mineral assemblage chloritoid, talc,

phengite, and quartz. Tiny sericitic phengite and chlorite crystals are locally found as retrograde products after chloritoid destabilization, attributed to the greenschist facies overprint. The transition between the whiteschist body toward the metagranite occurs on a small distance, over a few tens of centimeters to one meter, and is characterized by a completely retrogressed paragenesis, in which the peak pressure whiteschist paragenesis is replaced by a greenschist facies mineral assemblage consisting of chlorite, white mica, and quartz.

## ANALYTICAL METHODS

### X-ray fluorescence (XRF)

Fresh samples were selected and crushed with a hydraulic press. Rock fragments were powdered in a tungsten carbide mill, dried in the oven at 110 °C, and calcined at 1050 °C for 3 h. Loss on ignition (LOI) was calculated by weight difference after calcination. Powders were mixed with lithium tetraborate ( $\text{Li}_2\text{B}_4\text{O}_7$ ) and melted to produce glass pellets. The major element oxides were determined by X-ray fluorescence using a PANalytical Axios-mAX spectrometer at Lausanne University, Switzerland. Ferrous iron was determined by a colorimetric method at Lausanne University, Switzerland.

### Electron probe microanalyzer (EPMA)

White micas covering part of the phengite compositional range were selected and tested for chemical homogeneity in major elements by EPMA (Table 1). Si, Ti, Al, Mg, Fe, K, Na, Ca, F, and Cl content of white mica were measured using a JEOL JXA-8350F HyperProbe EPMA at Lausanne University, Switzerland. Operating conditions were 15 kV, 15 nA, and a beam size of 5  $\mu\text{m}$ . Natural minerals were used as standards. White mica structural formulas were obtained by normalization on a basis of 22 negative charges.

### Laser fluorination (LF) for oxygen isotope analysis

The oxygen isotope composition of white mica reference materials was determined at the University of Lausanne (Switzerland) using the  $\text{CO}_2$  laser fluorination technique (Lacroix and Vennemann 2015) coupled with a Thermo-Finnigan MAT 253 gas source mass spectrometer. White mica grain separates were loaded into Pt holders and dried in the oven at 110 °C for ca. 12 h before loading into the LF chamber. White mica SIMS reference materials were analyzed as replicates in several sessions. During each analytical session, white mica aliquots were measured together with the NBS-28 quartz. White mica data are corrected to the session value of the NBS-28 quartz [accepted value of 9.64‰ as reported by Coplen et al. (1983)]. The repeatability of NBS-28 quartz determined as the average of daily replicates is usually better than 0.1‰ (1 SD). Data are given in conventional  $\delta$ -notation, relative to Vienna Standard Mean Ocean Water (VSMOW).

### Thermodynamic modeling

The whiteschist 14MR67 whole-rock composition with the following composition determined by XRF is used for thermodynamic modeling:  $\text{SiO}_2$ : 66.13;  $\text{TiO}_2$ : 0.43;  $\text{Al}_2\text{O}_3$ : 15.85;  $\text{Fe}_2\text{O}_3$ : 1.75;  $\text{FeO}$ : 1.29;  $\text{MnO}$ : 0.02;  $\text{MgO}$ : 6.51;  $\text{CaO}$ : 0.17;  $\text{Na}_2\text{O}$ : 0.44;  $\text{K}_2\text{O}$ : 3.07;  $\text{P}_2\text{O}_5$ : 0.13;  $\text{H}_2\text{O}$ : 4.34. Since  $\text{CaO}$ ,  $\text{Na}_2\text{O}$ ,  $\text{TiO}_2$ ,  $\text{P}_2\text{O}_5$ , and  $\text{MnO}$  are only present in minor amounts (<0.5 wt%), the simplified KFMASH system was used for thermodynamic modeling. All iron was assumed to be ferrous. The composition used is (in moles):  $\text{SiO}_2$  (66.02),  $\text{AlO}_{1.5}$  (18.65),  $\text{FeO}$  (1.73),  $\text{MgO}$  (9.69),  $\text{KO}_{0.5}$  (3.91).  $\text{H}_2\text{O}$  saturated conditions were assumed since no carbonate phase was observed in this whiteschist. Initial calculations revealed that carbonates become stable with only minor amounts of  $\text{CO}_2$  in the fluid ( $X_{\text{CO}_2} < 0.1$ ), which do not significantly influence the *P-T* conditions calculated by dehydration reactions (Bucher-Nurminen et al. 1983). Calculations were performed using the internally consistent database of Berman (Berman 1988; 92 update) and Domino software (de Capitani and Brown 1987). Solution models used are from Berman (Berman 1988), except for white mica (Massonne and Szpurka 1997). To account for the small amount of iron measured in talc (average  $X_{\text{Mg}}$  of 0.95), we adjusted the standard state thermodynamic  $S^0$  of Mg-talc in Berman's thermodynamic data as follows:  $S_{\text{Fe-MgTlc}}^{0,90} = S_{\text{MgTlc}}^{0,90} - R \ln(a)$ , with  $S_{\text{Fe-MgTlc}}^{0,90}$  being the standard state entropy of Fe-Mg-talc at 25 °C and 1 bar,  $S_{\text{MgTlc}}^{0,90}$  is the standard state entropy of pure Mg-Talc,  $R$  is the gas constant and  $a$  is the activity of talc, calculated as:  $a = (X_{\text{Mg}})^2$ , with  $X_{\text{Mg}} = \text{Mg}/(\text{Mg}+\text{Fe})$ . The corrected standard state  $S^0$  is 262.5199 J/(K mol) for an average talc  $X_{\text{Mg}}$  of 0.95.

**TABLE 1.** Major and minor element composition (wt%) of white mica reference materials with structural formula (apfu)

Unil RM	Unil_WM1		Unil_WM2		Unil_WM3		Unil_WM4	
	Average (n = 25)	1SD*						
$\text{SiO}_2$	46.35	0.18	51.49	0.17	49.31	0.53	51.02	0.26
$\text{TiO}_2$	0.44	0.09	0.52	0.03	0.30	0.07	0.20	0.01
$\text{Al}_2\text{O}_3$	35.26	0.09	24.42	0.20	28.28	1.14	27.04	0.42
$\text{FeO}$	1.13	0.06	2.91	0.11	3.67	0.29	1.66	0.08
$\text{MgO}$	0.84	0.06	4.04	0.08	1.52	0.21	3.76	0.24
$\text{CaO}$	0.00	0.01	0.00	0.00	0.00	0.00	0.00	0.00
$\text{Na}_2\text{O}$	0.81	0.03	0.18	0.04	0.11	0.04	0.53	0.06
$\text{K}_2\text{O}$	10.58	0.05	11.33	0.05	11.58	0.10	11.05	0.12
F	0.15	0.04	0.00	0.00	0.00	0.00	0.00	0.00
Cl	0.00	0.00	0.00	0.00	0.00	0.00	0.00	0.00
Total	95.56		94.90		94.78		95.26	
Si (T)	3.082	0.012	3.479	0.011	3.350	0.036	3.407	0.018
Al (T)	0.918	0.012	0.521	0.011	0.650	0.036	0.593	0.018
sum T	4.000		4.000		4.000		4.000	
Ti (O)	0.022	0.005	0.027	0.002	0.016	0.003	0.010	0.001
Al (O)	1.845	0.015	1.424	0.010	1.615	0.058	1.536	0.025
Fe (O)	0.063	0.003	0.165	0.006	0.208	0.016	0.093	0.005
Mg (O)	0.084	0.006	0.407	0.008	0.154	0.021	0.374	0.024
Mn (O)	0.000	0.000	0.000	0.000	0.000	0.000	0.000	0.000
Cr (O)	0.000	0.000	0.000	0.000	0.000	0.000	0.000	0.000
Ni (O)	0.000	0.000	0.000	0.000	0.000	0.000	0.000	0.000
sum O	2.013		2.022		1.993		2.013	
Ca (A)	0.000	0.000	0.000	0.000	0.000	0.000	0.000	0.000
Na (A)	0.104	0.004	0.024	0.005	0.015	0.005	0.068	0.008
K (A)	0.897	0.005	0.976	0.005	1.003	0.009	0.941	0.010
sum A	1.002		1.000		1.018		1.010	

Note: Calculated on a basis of 22 charges.

\* Uncertainty expressed as 1SD.

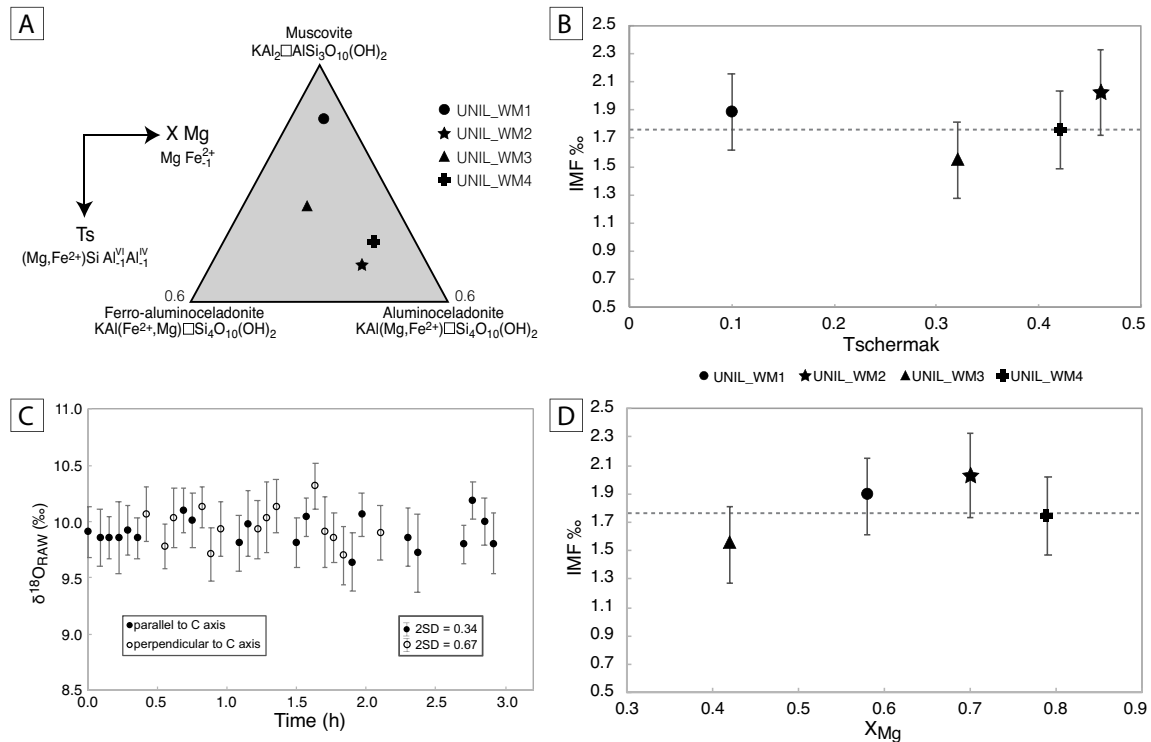


**FIGURE 2.** (a) Potassium white mica classification triangle of Rieder et al. (1999), showing the muscovite end-member and the theoretical aluminoceladonite and ferro-aluminoceladonite end-members. The triangle displays the potential compositional range of natural phengites (Guidotti and Sassi 1998). Solid symbols are the compositions of the white mica reference materials (RMs) developed in this study. (b) A plot of instrumental mass fractionation (IMF) as a function of the Tschermak exchange vector  $[Si^{IV}(Mg,Fe)^{VI} \leftrightarrow Al^{IV}Al^{IV}]$  for the RMs. The IMF is calculated as:  $IMF = \delta^{18}O(SIMS) - \delta^{18}O$  (laser fluorination). (c) Orientation test performed on three grains of UNIL\_WM1. One grain was oriented such that the analyses were performed parallel to the C axis, the two others were oriented for analysis perpendicular to the C axis. Error bars indicate 2SE, i.e., two times the standard error on the mean of the 20 cycles measured for each data point. Note that no IMF bias was detected between different white micas, however the large scatter in  $\delta^{18}O$  in the crystals oriented perpendicular to the C axis is due to their thin width and the presence of some epoxy between the mica sheets, therefore some analyses could include a small amount of epoxy. (d) Finally, IMF was plotted vs.  $X_{Mg}$ . At the level of the precision of measurement of ca. 0.4% 2SE it is not possible to see a compositional dependence of the IMF, since the largest and the smallest values determined differ by 0.58‰ (see text for details).

### Secondary ion mass spectrometry (SIMS)

White mica reference materials were mounted and polished in epoxy mounts together with the biotite standard UNIL\_B2 (Siron et al. 2017) for drift monitoring. The topography of the mounts was systematically checked using a white light interferometer and a maximum of 5  $\mu m$  relief accepted. Epoxy and indium mounts were cleaned using pure ethanol, dried in the oven at 60 °C and stored in a vacuum desiccator. They were coated with 35 nm of gold.

In situ oxygen isotopes measurements were conducted on a Cameca IMS 1280HR instrument in the SwissSIMS facility (University of Lausanne, Switzerland), using a focused high-density 1.5 nA Cs<sup>+</sup> primary beam at 10 kV in a Gaussian mode. A spot size of ~15  $\mu m$  was achieved without rastering. An electron flood gun was used to compensate surface charge and was optimized before each session. An entrance slit of 122  $\mu m$  and exit slit of 1346  $\mu m$  allowed a mass resolution of ~2400. <sup>16</sup>O and <sup>18</sup>O were measured simultaneously in multi-collection mode on Faraday cups. Mass calibration, background correction, and Faraday cups calibration were performed at the beginning of each session. Counting statistics on 20 acquisition cycles for each analysis gave an uncertainty precision in the order of 0.20 to 0.35‰ (2 standard errors, noted hereafter 2SE). A typical session was set with 4–6 UNIL\_B2 standard analyses at the beginning, followed by one standard analysis between each three unknowns, to monitor drift. Drift was corrected if needed by applying first- or second-order polynomial regressions based on the fit of reference material analyses. Intra-grain and inter-grain oxygen isotope variability of the reference materials was tested on a total of 5 to 10 grains from each species, randomly selected, by measuring 3 to 20 SIMS spot analyses on different regions within each grain (Online Materials<sup>1</sup> OM1).

To determine any compositional related instrumental mass fractionation (IMF), several grains of each species were mounted together in the same mount and measured in a calibration session with one of the reference materials as internal standard. Data were corrected for drift when needed. If the IMF is small (<20‰), it can be formulated following Equation 1 (Eiler et al. 1997; Siron et al. 2017):

$$IMF(\text{‰}) = \delta^{18}O_{SIMS} - \delta^{18}O_{LF} \quad (1)$$

Here,  $\delta^{18}O_{SIMS}$  is the mean of measurements in a session of a reference material SIMS measurements, corrected for drift if necessary, and  $\delta^{18}O_{LF}$  is the mean of all laser fluorination (LF) measurements for a given sample. IMF is calculated for each reference material and the  $\Delta IMF$  is then calculated as the difference between the maximal and minimal IMF value among the four reference materials. The details of the development of the RM materials are discussed below.

The Monte Rosa thin sections were analyzed together with the newly established white mica reference material UNIL\_WM3 ( $7.9 \pm 0.09\text{‰}$ ) and quartz reference material UNIL-Q1 ( $9.8 \pm 0.06\text{‰}$ ; Seitz et al. 2017). Thin sections chips were pressed in indium together with cut epoxy pieces containing a polished white mica RM and a polished quartz RM. White mica and quartz  $\delta^{18}O$  were measured in two different sessions, both using a primary beam of 1.5 nA, without raster.

Final uncertainty on each unknown SIMS measurement was calculated following Equation 2:

$$2SE = \sqrt{(2SE_{SIMS}^{unk})^2 + (2SD_{SIMS}^{RM})^2 + (2SD_{LF}^{RM})^2} \quad (2)$$

Where  $2SE_{\text{SIMS}}^{\text{unk}}$  represents two times the standard error on the mean of the 20 cycles measured for each SIMS analyses,  $2SD_{\text{SIMS}}^{\text{RM}}$  is two times the standard deviation on the mean of the  $n$  analyses of the reference material used to calibrate SIMS measurements, and  $2SD_{\text{RM}}^{\text{ref}}$  is two times the standard deviation (SD) on the reference value of the reference material obtained by laser fluorination. The typical uncertainty on each single unknown analysis is in the order of 0.2 to 0.3‰ (2SE), and the uncertainty on the reference materials is 0.33‰ (2SD) for UNIL\_WM3 and 0.26‰ (2SD) for UNIL\_Q1.

### WHITE MICA REFERENCE MATERIAL (RM) FOR IN SITU OXYGEN ISOTOPE ANALYSIS

#### Chemical and oxygen isotope homogeneity tests of RMs

The chemical variability of the white mica samples is assessed through the relative error based on the standard deviation of the mean for major elements (1SD), as well as the standard deviation of the mean on the oxygen isotope composition (2SD). Four white mica species, among them one muscovite (UNIL\_WM1) and three phengites (UNIL\_WM2, UNIL\_WM3, and UNIL\_WM4) were selected since they have acceptable chemical (<2% relative for Al, Si, K and <7% relative for Mg and Fe) and isotopic (<0.40‰ 2SD) variations within grain and between grains (Fig. 2). One white mica sample (UNIL\_WM3) shows a slightly higher chemical variability (4% relative for Al and 14% relative for Mg). UNIL\_WM1 consists of several large crystals from a Brazilian mica schist sample, and UNIL\_WM2 are large crystals from a Himalayan mica schist sample, and UNIL\_WM3, as well as UNIL\_WM4, are crushed separates from Alpine rocks. The white mica RMs cover the compositional range from 3.08 to 3.48 Si pfu and an  $X_{\text{Mg}}$  from 0.43 to 0.80 (Table 1; Fig. 2a).

The typical repeatability of SIMS oxygen isotope measurements on three to six points in individual white mica grains is between 0.30 and 0.40‰ (2SD) (Online Materials<sup>1</sup> Table OM1). White mica is notoriously difficult to polish, and the reproducibility of SIMS measurement is highly dependent on the quality of the polishing. Laser fluorination  $\delta^{18}\text{O}$  values are:  $10.4 \pm 0.06\text{‰}$  for UNIL\_WM1,  $5.6 \pm 0.04\text{‰}$  for UNIL\_WM2,  $7.9 \pm 0.09\text{‰}$  for UNIL\_WM3 and  $5.3 \pm 0.17\text{‰}$  for UNIL\_WM4 (Table 2).

#### Instrumental mass fractionation

Two mounts containing all RMs were used to test for compositional variations of instrumental mass fractionation (IMF). Four calibration sessions were performed with varying analysis conditions (i.e., primary beam of 1, 1.5, and 2 nA; with a 10  $\mu\text{m}$  raster and without raster), to reduce the IMF and find the optimal analytical conditions. A  $\Delta\text{IMF}$  of 0.24‰ was achieved with the optimal analytical conditions of 1.5 nA primary beam, without raster (Online Materials<sup>1</sup> OM2). Other analytical conditions gave  $\Delta\text{IMF}$  between 0.58 and 0.71‰. Plots of IMF vs. major element compositions were tested (Tschermak exchange vector and  $X_{\text{Mg}}$ ; Figs. 2b–2d) to detect any compositionally dependent mass fractionation. However, no relationship between major element composition and IMF was found in the different sessions, even though there is a linear IMF dependency on  $X_{\text{Mg}}$  for biotite (Siron et al. 2017). In fact, the chemical variations in white mica are small when compared with biotite, which has a large Mg and Fe variation, for instance. An orientation test was performed in order to evaluate IMF due to crystal orientation. One crystal was oriented parallel to the  $c$ -axis, and two others

**TABLE 2.** Oxygen isotope composition of white mica reference materials by laser fluorination together with the NBS-28 quartz standard

Unil RM Date	Unil_WM1		
	Corrected $\delta^{18}\text{O}$ ‰	1 SD <sup>a</sup>	$n$
15-April-2016	10.43	$\pm 0.10$	1
16-April-2016	10.36	$\pm 0.01$	2
28-October-2016	10.36	$\pm 0.10$	2
Average	10.37	$\pm 0.06$	5
UNIL_RM	UNIL_WM2		
	corrected $\delta^{18}\text{O}$ ‰	1 SD <sup>a</sup>	$n$
16-April-2016	5.67	$\pm 0.10$	1
21-March-2018	5.63	$\pm 0.04$	3
Average	5.64	$\pm 0.04$	4
UNIL_RM	UNIL_WM3		
	corrected $\delta^{18}\text{O}$ ‰	1 SD <sup>a</sup>	$n$
15-April-2016	7.85	$\pm 0.05$	2
21-March-2018	7.98	$\pm 0.08$	2
Average	7.91	$\pm 0.09$	4
UNIL_RM	UNIL_WM4		
	corrected $\delta^{18}\text{O}$ ‰	1 SD <sup>a</sup>	$n$
15-April-2016	5.40	$\pm 0.25$	2
28-October-2016	5.23	$\pm 0.02$	2
Average	5.32	$\pm 0.17$	4
Standard	NBS-28 quartz standard		
	$\delta^{18}\text{O}$ ‰	1 SD <sup>a</sup>	$n$
15-April-2016	9.86	$\pm 0.05$	3
16-April-2016	9.51	$\pm 0.11$	4
28-October-2016	9.56	$\pm 0.03$	3
21-March-2018	9.49	$\pm 0.02$	5

<sup>a</sup>Uncertainty is expressed as 1 SD.

were oriented perpendicular to the  $c$ -axis. No IMF change was detected (Fig. 2c). Difficulties were encountered for the samples mounted parallel to  $c$  due to the small thickness of the crystals, which resulted in a small exposed surface, reducing the reproducibility. Nevertheless, these results are in agreement with tests performed on biotite by Siron et al. (2017), who did not find any orientation-dependent fractionation effect. Despite the lack of obvious compositional dependencies for white mica, we recommend using the RM, which is chemically closest to that of the compositions of white micas to be measured.

### APPLICATION TO WHITESCHIST AND METAGRANITES FROM THE MONTE ROSA NAPPE

#### Sample description

Three samples were selected for detailed SIMS work: two metagranites and one whiteschist. Sample 16MR23 is an undeformed porphyritic metagranite, called metagranite 1 in this study (Fig. 3a). It contains igneous, centimeter-sized K-feldspar phenocrysts, plagioclase, quartz, biotite, and muscovite. Metamorphic phengite overgrows igneous muscovites and is also found as biotite pseudomorphs, in association with titanite  $\pm$  garnet. Late biotite flakes surround those biotite pseudomorphs. Igneous plagioclase is nearly completely pseudomorphosed by a fine-grained assemblage of zoisite, albite, and white mica (Luisier et al. 2019). The cores of the plagioclase pseudomorphs are fine-grained, whereas the rims were recrystallized into a coarser-grained assemblage of Fe-rich clinzoisite, oligoclase, and white mica. Accessory phases are zircon, apatite, monazite, and ilmenite.

Sample 14MR25 is a little deformed porphyritic metagranite, called metagranite 2 in this study (Fig. 3b). It also contains centimeter-sized igneous K-feldspar phenocrysts. Igneous

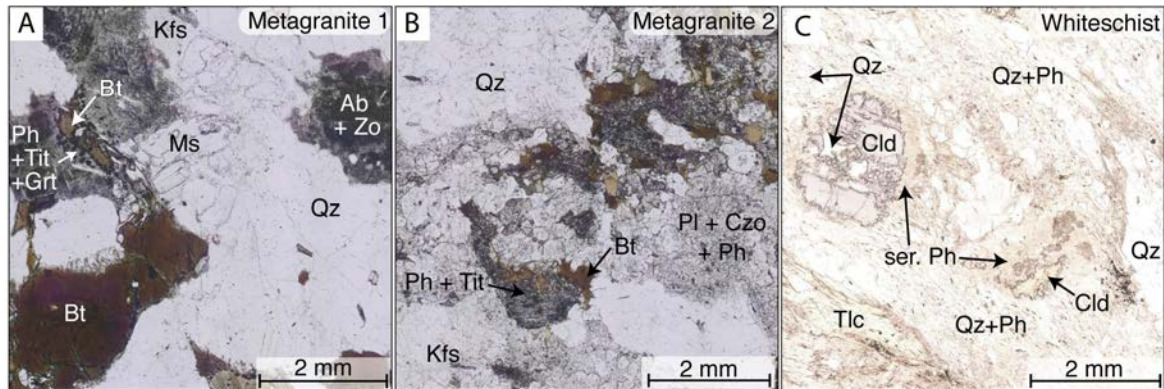


**FIGURE 3.** Thin sections photomicrographs in plane-polarized light illustrating the main petrographic characteristics of the samples investigated. (a) Metagranite 1 is an undeformed porphyritic K-feldspar metagranite, with igneous biotite, muscovite, quartz, and K-feldspar. Igneous plagioclase is pseudomorphosed by a fine-grained assemblage of albite + zoisite. Phengite + titanite + garnet form a reaction rim around biotite, when in contact with plagioclase pseudomorphs. (b) Metagranite 2 shows a more pronounced transformation, leaving only quartz and K-feldspar as igneous phases. Plagioclase was replaced by albite + clinozoisite + phengite. Biotite is completely replaced by a fine-grained assemblage of phengite and titanite, locally rimmed by retrograde biotite. (c) The whiteschist is composed of chloritoid, talc, phengite, and quartz. A slight foliation is marked by the phengite. Chloritoid is partially replaced by a fine-grained assemblage of sericitic phengite and chlorite. Mineral abbreviations are: Ab = albite; Bt = biotite; Cld = chloritoid; Czo = clinozoisite; Grt = garnet; Kfs = K-feldspar; Ms = muscovite; Ph = phengite; Pl = plagioclase; ser. Ph = sericitic phengite; Tlc = talc; Tit = titanite; Zo = zoisite. (Color online.)

plagioclase is replaced by an assemblage of clinozoisite, albite, and phengite. Igneous quartz is recrystallized into fine-grained, seriate, interlobate quartz, and igneous biotite is totally replaced by a fine-grained assemblage of phengite and titanite. Late, small biotite flakes surround those phengites. Small garnets can be found in association with plagioclase in domains close to former igneous biotite. Chlorite locally replaces the late biotite crystals. Accessory phases are titanite, zircon, apatite, monazite, and ilmenite.

Metagranite 1 is located about 80 m and metagranite 2 about 100 m away from the whiteschist outcrop, and both show little-to-no deformation. The study area is affected by a late deformation event associated with the exhumation of the Monte Rosa nappe. The deformation is observed as localized shear zones in the metagranite, separating large portions of nearly undeformed metagranite. The relationships between microstructures and mineral assemblage in the deformed metagranites indicate that deformation is related to the greenschist facies overprint, which post-dates peak pressure conditions. This is corroborated by the relative chronology of the deformation and crystallization relationships in the whiteschist, confirming a post (PT) peak deformation event throughout the studied area (see also Vaughan-Hammon et al. 2021).

The whiteschist sample 14MR67 (Fig. 3c) was collected close to the center of the whiteschist pipe. The sample contains big, dark blue chloritoid crystals embedded in a matrix of talc, phengite, and quartz. This paragenesis is characteristic of the Alpine high-pressure peak metamorphic conditions (Chopin and Monié 1984; Le Bayon et al. 2006; Luisier et al. 2019). A slight schistosity is defined by phengite and talc, which are deformed, indicating that the peak mineral assemblage is pre-kinematic relative to this light deformation. The deformation is associated with exhumation (e.g., Pawlig and Baumgartner 2001). Chlorite and sericitic phengite are found as fine-grained retrograde

products, which statically replace chloritoid as rims. Talc is partially replaced by chlorite. The fine-grained sericitic phengite and chlorite are post-kinematic relative to the main schistosity. Microstructural observations allow us to distinguish at least two distinct generations of white mica. The first generation of phen-

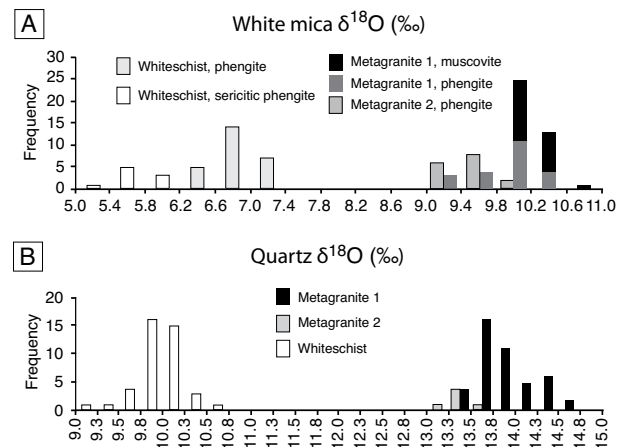


**FIGURE 4.** Histograms of  $\delta^{18}\text{O}$  values measured in white mica (a) and quartz (b) in different microstructural domains of the metagranite 1, metagranite 2, and the whiteschist. Analyses of igneous muscovite (metagranite 1) and phengites (metagranites 1 and 2) show different values. Note the pronounced difference of isotopic composition of high-pressure phengites and retrograde sericitic phengite in whiteschist. The range of each class corresponds to the standard deviation (2SD) of the reference materials analyses, corresponding to 0.34‰ in phengite and 0.26‰ in quartz. Whiteschist has—both in white mica and quartz—a significantly lower oxygen isotopes composition than the metagranites, which are the protoliths for the whiteschist (Luisier et al. 2021). Metagranite 1 and 2 show overlapping  $\delta^{18}\text{O}$  compositions, however, in metagranite 2 the  $\delta^{18}\text{O}$  values are at the lower range of the metagranite spectrum.

gites deformed locally in the main schistosity and belonged to the high-pressure paragenesis. The second generation is formed by the fine-grained sericitic phengites, replacing chloritoid on its rim. This retrograde alteration is greenschist facies. Quartz grains are present either as big crystals (Fig. 3c) with sub-grain boundaries reflecting incipient deformation or as small crystals within the mica-rich domains in the schistosity, or as inclusions in chloritoid. Accessory minerals are zircon, apatite, allanite, rutile, monazite, xenotime, and florencite.

### Oxygen isotope composition of quartz and phengite

The  $\delta^{18}\text{O}$  values of igneous muscovite in the metagranite 1 show a range between 9.8 and 10.7‰ (Fig. 4a), which is slightly higher than the reference material typical reproducibility of 0.4‰ (2SD). Metamorphic phengites  $\delta^{18}\text{O}$  values are slightly less enriched in  $^{18}\text{O}$  (9.1–10.4‰). The  $\delta^{18}\text{O}$  range of metamorphic phengite in both metagranite 1 and metagranite 2 is similar. Phengites from whiteschists are characterized by lower  $\delta^{18}\text{O}$  values (5.2–7.3‰) when compared to the two metagranites, and the range in values is larger. Here, two distinct populations can be correlated with microtextures. The first population is represented by large phengite flakes with  $\delta^{18}\text{O}$  values > 6‰ (Fig. 5a).

The second population is the smaller sericitic phengite crystals, typically replacing chloritoid. This generation is younger than the large flakes and grows during retrograde chloritoid breakdown. They have  $\delta^{18}\text{O}$  values < 6‰. The sericitic phengites are typically isolated from quartz crystals.

Quartz  $\delta^{18}\text{O}$  values in the metagranite 1 range from 13.4 to 14.6‰ (Fig. 4b). This is outside the reference material typical reproducibility of 0.3‰ (2SD). Indeed, the centers of the larger grains, interpreted to be igneous, cluster toward the lower values of that range and the smaller, recrystallized grains, as well as the outer parts of the larger grains, are closer to the upper end of the  $\delta^{18}\text{O}$  range (Fig. 5b). Fine-grained quartz crystals from the metagranite 2 are homogeneous within uncertainty with values between 13.2 and 13.5‰. Whiteschist quartz has  $\delta^{18}\text{O}$  values ranging from 9.1 to 10.6‰. No correlation with microtexture was found (Fig. 5a).

The  $\delta^{18}\text{O}$  values of white micas were plotted against their silica content for each white mica generation in Figure 6a. Large muscovites, interpreted to be igneous in metagranite 1 have silica contents ranging between 3.01 and 3.14 atoms per formula unit (apfu). They are homogeneous within uncertainty and show the highest  $\delta^{18}\text{O}$  values. One data point is slightly higher. Metamorphic phengites from metagranite 1 have compositions ranging from 3.03 to 3.17

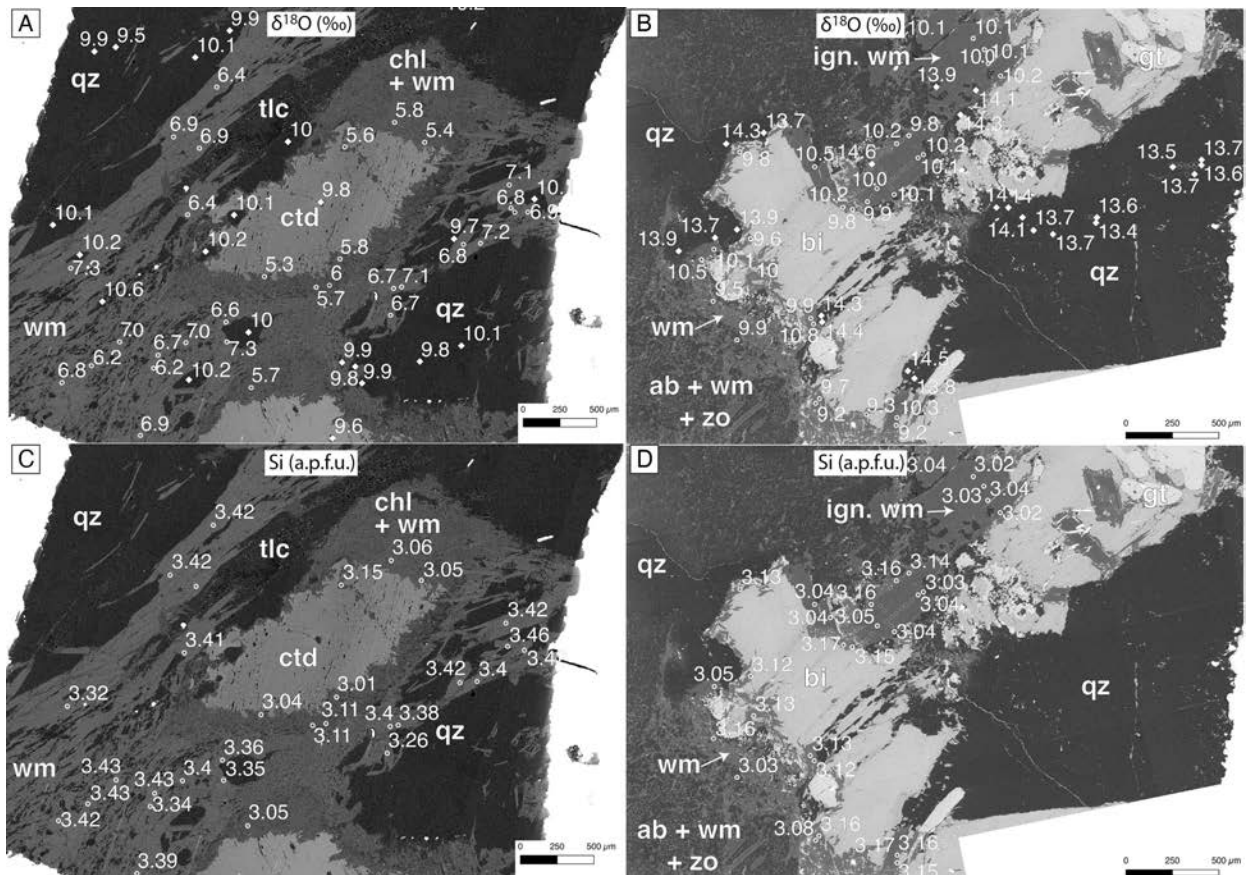


**FIGURE 5.** SIMS  $\delta^{18}\text{O}$  data in ‰ for white mica (dots) and quartz (diamonds) are plotted onto BSE images. Also given is the silica content per formula unit (apfu) of white mica. (a)  $\delta^{18}\text{O}$  of white mica and quartz from the whiteschist (sample 14MR67) (b)  $\delta^{18}\text{O}$  (‰) of white mica and quartz from the metagranite 1 (sample 16MR23) (c) Si (apfu) content of white mica in whiteschist (14MR67) (d) Si (apfu) content of white mica in metagranite 1. Large igneous white micas have metamorphic overgrowths of fine grains. Mineral abbreviations are: ab = albite; bi = biotite; chl = chlorite; ctd = chloritoid; gt = garnet; ign. wm = igneous white mica; qz = quartz; tlc = talc; wm = white mica; zo = zoisite.

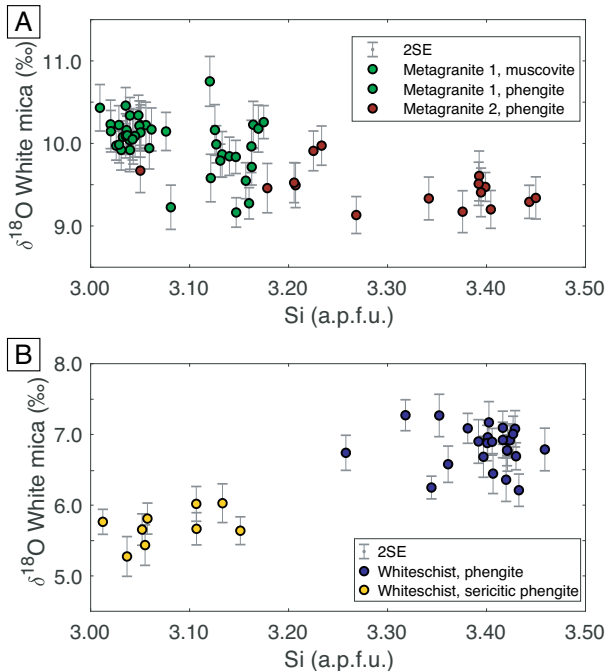


**FIGURE 6.** White mica oxygen isotope composition was plotted against the silica content of white mica (apfu): for (a) metagranite 1 and 2 and (b) whiteschist. Error bars indicate the uncertainty of each measurement, expressed as 2SE (%). Note the isotopic compositions of phengite do not correlate with phengite contents in the metagranites, in contrast to a well distinguished change in composition in the whiteschists. Two different groups are defined in the whiteschist, in chemical composition and in isotope composition. (Color online.)

silica apfu, which is identical to igneous muscovites. However, they show a wider range in  $\delta^{18}\text{O}$  values, without a correlation with celadonite composition (Figs. 5b and 5d). The silica content of phengites in the metagranite 2 are higher than those in metagranite 1 and lie (with one exception) between 3.20 and 3.45 apfu (Fig. 6a). They have the lowest  $\delta^{18}\text{O}$  value among metagranites, but no clear correlation between Si content and  $\delta^{18}\text{O}$  was observed. Hence, there is no correlation of  $\delta^{18}\text{O}$  values with celadonite (e.g., silica) content. The celadonite component is a monitor of pressure at which the phengite formed in granitic mineral assemblages since the buffer assemblage quartz-K-feldspar-biotite-phengite is present in these granites (e.g., Massonne and Schreyer 1987).

The oxygen isotopic composition of phengite in whiteschist is plotted as a function of silica content in Figure 6b. Two groups are visible, low-silica content phengites plot around a  $\delta^{18}\text{O}$  value of 5.2–6.0‰, while high-silica content phengites plot between 6.1–7.2‰. These two groups are reflected in the histograms in Figure 4a. As outlined above, the low-silica phengites are crystals measured in the retrograde sericitic phengite haloes surrounding the chloritoid (see also Figs. 5a and 5c). Interestingly, there is no dependence of the  $\delta^{18}\text{O}$  value on the silica content of the phengites within each group.

### White mica-quartz isotope thermometry

Temperatures have been calculated, based on the fractionation between quartz and muscovite and quartz and phengite (Zheng

1993) for quartz-white mica pairs (Fig. 7) from the same microstructural domains (Table 3).

In metagranite 1, quartz-white mica pairs can be separated into two populations: igneous muscovite and quartz pairs and metamorphic phengite and quartz pairs. Igneous pairs result in oxygen isotope fractionation temperatures between 350 and 450 °C (Table 3; Fig. 7). These values are clearly too low for igneous crystallization temperatures and most likely reflect subsolidus re-equilibration during cooling of the granite intrusion as is often seen in granitic systems (see, e.g., O'Neil et al. 1977) or metamorphic re-equilibration upon cooling after the Alpine metamorphism (see, e.g., Eiler et al. 1993). The metamorphic overgrowths and fine-grained phengites in the matrix were paired with the rims of igneous quartz and recrystallized quartz grains and indicate a temperature range of 300 to 330 °C (Fig. 7). Using this temperature range and the phengite content of these mica crystals (3.03 to 3.17; Table 3) results in pressures of <0.2 GPa, assuming a  $\text{H}_2\text{O}$  activity of 1 (Massonne and Szpurka 1997). The temperature and pressure range for these metamorphic phengites in metagranite 1 suggests a prehnite-actinolite or low-temperature greenschist facies.

Metagranite 2 is characterized by metamorphic phengites, replacing igneous biotites. The pseudomorphic nature of these domains and the juxtaposition of the pseudomorphs with plagioclase did not allow us to find many quartz-phengite pairs that can be assumed to be in isotopic equilibrium based on textural arguments. Nevertheless, a pair with high-silica phengite (3.39 apfu) was identified, suggesting it to be a high-pressure mica. It yields a temperature of  $350 \pm 40$  °C (Table 3). The temperature obtained is similar to (within uncertainty) low-silica phengite

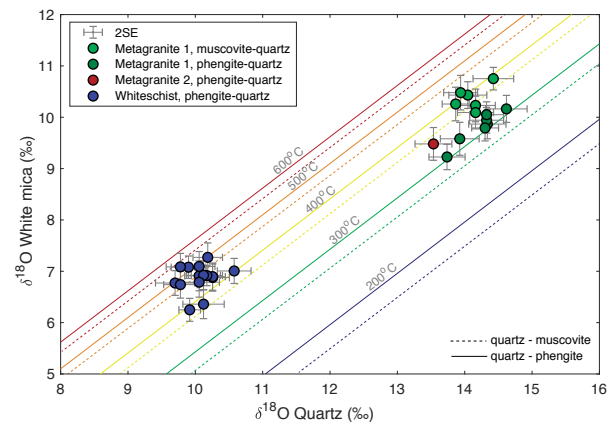


**FIGURE 7.**  $\delta^{18}\text{O}$  of quartz vs.  $\delta^{18}\text{O}$  of white mica plotted for pairs of white mica and quartz, measured in selected microstructural domains where the mineral pairs belong to the same textural domains. Error bars show the uncertainty (2SE). Temperature isolines were calculated based on the fractionation coefficients between quartz and phengite (solid lines; Zheng 1993) as well as quartz and muscovite (dashed lines; Zheng 1993). The whiteschist pairs define a tight cluster around 450 °C. The size of the cluster is mainly defined by analytical uncertainties. Only data for high-pressure phengites could be used, since no quartz is found in the retrograde alteration rims of chloritoid. Note that metagranite 1 phengite-quartz pairs display a weak trend parallel to the isolines, suggesting that isotopic equilibrium seems to have been attained between  $\delta^{18}\text{O}$  of quartz and white mica at a temperature of ca. 350 °C. (Color online.)

**TABLE 3.** White mica and quartz SIMS data used as pairs for temperature calculation, based on the quartz-muscovite and quartz-phengite fractionation coefficients from Zheng (1993)

White mica	Species	Si (apfu)	$\delta^{18}\text{O}$ (‰)	2SE <sup>a</sup>	Quartz	$\delta^{18}\text{O}$ (‰)	2SE <sup>a</sup>	T (°C)	± (°C)
<b>Metagranite 1</b>									
16MR23@31	muscovite	3.02	10.2	0.29	16MR23_qz@05	14.2	0.32	403	48
16MR23@35	muscovite	3.01	10.4	0.28	16MR23_qz_2@05	14.1	0.26	443	50
16MR23@47	muscovite	3.05	9.2	0.27	16MR23_qz@13	13.7	0.25	343	34
16MR23@48	muscovite	3.03	10.5	0.25	16MR23_qz@14	13.9	0.34	463	59
16MR23@30	muscovite	3.12	10.8	0.30	16MR23_qz_2@1	14.4	0.22	435	48
16MR23@40	muscovite	3.17	10.3	0.20	16MR23_qz_2@04	13.9	0.33	443	50
16MR23@32	muscovite	3.04	10.1	0.27	16MR23_qz@05	14.2	0.32	387	46
<b>Average temperature of igneous muscovites</b>								<b>404</b>	<b>42</b>
16MR23@36	phengite	3.06	9.9	0.25	16MR23_qz_2@06	14.3	0.25	317	33
16MR23@38	phengite	3.04	10.1	0.25	16MR23_qz_2@06	14.3	0.25	326	34
16MR23@16	phengite	3.13	10.2	0.31	16MR23_qz_2@09	14.6	0.26	310	36
16MR23@25	phengite	3.13	9.8	0.20	16MR23_qz@10	14.3	0.25	305	28
16MR23@26	phengite	3.12	9.6	0.29	16MR23_qz@11	13.9	0.32	320	40
16MR23@29	phengite	3.13	9.9	0.28	16MR23_qz_2@02	14.3	0.29	309	35
<b>Average temperature of metamorphic phengites</b>								<b>314</b>	<b>8</b>
<b>Metagranite 2</b>									
14MR25@19	phengite	3.39	9.5	0.27	14MR25_qz@2	13.5	0.32	349	43
<b>Whiteschist</b>									
14MR67@19	phengite	3.26	6.7	0.25	14MR67_qz@16	9.8	0.26	477	57
14MR67@36	phengite	3.32	7.3	0.22	14MR67_qz@06	10.2	0.28	498	61
14MR67@40	phengite	3.34	6.3	0.16	14MR67_qz@18	9.9	0.22	391	34
14MR67@21	phengite	3.38	7.1	0.21	14MR67_qz@16	9.8	0.26	537	64
14MR67@29	phengite	3.40	6.9	0.25	14MR67_qz@12	10.3	0.26	428	49
14MR67@30	phengite	3.41	6.9	0.19	14MR67_qz@12	10.3	0.26	430	45
14MR67@33	phengite	3.42	6.4	0.31	14MR67_qz@10	10.1	0.28	380	48
14MR67@31	phengite	3.42	6.9	0.23	14MR67_qz_2@10	10.2	0.20	446	43
14MR67@34	phengite	3.42	6.9	0.25	14MR67_qz@10	10.1	0.28	453	56
14MR67@25	phengite	3.42	6.9	0.22	14MR67_qz@13	10.1	0.29	462	55
14MR67@26	phengite	3.42	7.1	0.23	14MR67_qz@13	10.1	0.29	490	61
14MR67@22	phengite	3.42	6.8	0.29	14MR67_qz@14	9.7	0.24	495	64
14MR67@32	phengite	3.43	7.1	0.26	14MR67_qz@11	9.9	0.22	514	60
14MR67@37	phengite	3.43	7.0	0.25	14MR67_qz@05	10.6	0.24	403	44
14MR67@24	phengite	3.46	6.8	0.30	14MR67_qz@13	10.1	0.29	443	60
<b>Average temperature of phengites with <math>3.38 \leq \text{Si (apfu)} \leq 3.46</math></b>								<b>443</b>	<b>46</b>

<sup>a</sup> Uncertainty expressed as 2SE.

from metagranite 1 (Fig. 7). The maximum silica content of the phengite (3.45 apfu) requires pressures of ca. 0.5 GPa at 350 °C (Massonne and Szpurka 1997). In contrast, if these phengites were formed during peak temperature of 575 °C, as proposed by Luisier et al. (2019), this would correspond to a pressure of 1.1 GPa (Massonne and Szpurka 1997). Then, the temperatures calculated from oxygen isotope thermometry would also reflect retrograde re-equilibration of the small mica crystals by diffusion upon cooling during the regional Alpine event. The slightly lower temperatures obtained for the small metamorphic crystals would agree with this suggestion (Eiler et al. 1993).

White micas in the whiteschist used for temperature estimation are the high-pressure phengites (Si > 3.38 apfu). The results span a rather large temperature range with an average of 440 ± 50 °C (Table 3; Fig. 7). The large variation is due to two effects. On one hand, white mica and quartz oxygen isotope data showed variabilities of 0.7 and 0.9‰, respectively. On the other hand, uncertainties accumulated by SIMS analysis (0.3‰ for phengite, 0.3‰ for quartz), together with the small temperature dependence of the white mica-quartz fractionation for oxygen isotopes, will also lead to large uncertainties of ca. ±50 °C (assuming an uncertainty of 0.4‰ for the oxygen isotope fractionation measurement). This temperature range partially overlaps with previous temperature estimates of prograde to peak Alpine metamorphic conditions from the literature (500–575 °C; Chopin and Monié 1984; Le Bayon et al. 2006; Luisier et al. 2019;

Vaughan-Hammon et al. 2021). Slightly lower oxygen isotope temperature compared to the peak temperature conditions from the literature could be explained by diffusive re-equilibration during post-peak, retrograde cooling.

The temperature of the retrograde growth event of the younger white mica generation replacing chloritoid cannot be determined by using quartz and white mica pairs, since quartz is absent from the pseudomorphs. Nevertheless, chlorite-phengite parageneses are typical for greenschist metamorphism (300–450 °C; Bucher and Grapes 2011).

## DISCUSSION

### Formation of the whiteschist protolith and its Alpine metamorphic evolution

White mica and quartz oxygen isotope compositions show a significant variation between the whiteschist and metagranite samples, showing that the igneous isotopic compositions were completely reset during metasomatism of the granite to produce the whiteschist protolith. Pawlig and Baumgartner (2001) suggested an argillitic alteration of the Monte Rosa granite by late magmatic fluids, producing the chemistry of the whiteschist protolith by producing a rock composed of sericite, chlorite, and quartz. The pre-Alpine age of the metasomatic alteration has been confirmed by Marger et al. (2019), based on the study of chemical and isotopic zoning patterns recorded in tourmaline

from whiteschists. Different conclusions were reached by Sharp et al. (1993), based on oxygen isotope data on bulk mineral separates from the Dora Maira whiteschist. They suggested a metasomatizing fluid of seawater origin, which was liberated by dehydration of serpentinite. However, the implication of fluids related to the dehydration of mafic to ultramafic rocks in the genesis of the whiteschist protolith has been discussed by Luisier et al. (2021) in detail, based on the geometry of alteration, the major element and stable isotope composition of bulk rocks, as well as stable isotope information presented in Marger et al. (2019). They confirmed the origin of the fluids to be hydrothermal, pre-high pressure, in the case of the Monte Rosa whiteschist genesis (Luisier et al. 2021).

The difference in isotopic composition for low- and high-silica phengites shown in Figure 6b for whiteschist documents a second alteration event, which leads to the formation of the retrograde replacement of chloritoid by white mica. Indeed, the high-pressure mineralogy of the whiteschist was acquired during the Alpine eclogite-facies metamorphism (Chopin and Monié 1984; Le Bayon et al. 2006; Luisier et al. 2019), inheriting the isotopic and chemical composition of the metasomatized granite. Quartz and chlorite reacted during the prograde increase in  $P$ - $T$  to form talc and chloritoid. This reaction consumes all chlorite over a relatively small  $P$ - $T$  range (see Fig. 8a). In parallel, the celadonite content increased, resulting in a maximum silica content of 3.46 apfu in phengite, in agreement with the isopleths calculated in the stability field of white mica-chloritoid-talc-quartz under

$\text{H}_2\text{O}$  saturated conditions (Fig. 8a). Calculations under  $\text{H}_2\text{O}$ -saturated conditions are justified due to the fact that the prograde reactions produce  $\text{H}_2\text{O}$  (Fig. 8b), a fact pointed out by Luisier et al. (2019); and supported by  $\text{H}_2\text{O}$  content measurements by SIMS in the high-pressure phengites by Luisier et al. (2019).

Decompression and cooling of the whiteschist will desiccate the grain boundaries. The fact that the peak assemblage is generally well-preserved shows that the retrograde chlorite breakdown reaction to biotite was never crossed. The chlorite to biotite breakdown reaction is a dehydration reaction, producing significant amounts of  $\text{H}_2\text{O}$  as indicated by the rapid drop in  $\text{H}_2\text{O}$  contained in the assemblage (Fig. 8b). Hence decompression was not accompanied by significant heating. Isothermal decompression or cooling during decompression is indicated by the preservation of the whiteschist peak assemblage. The localized, sericitic, low-celadonite phengites surrounding chloritoid require minor infiltration of external fluids. The texture suggests that chloritoid replacement by sericitic phengite happens simultaneously with local chloritization of talc. This retrograde replacement is related to a very localized fluid infiltration. The  $\delta^{18}\text{O}$  values of the late sericitic phengites are systematically about 1‰ lower than the high-pressure phengites (Fig. 6b). The fact that the quartz oxygen isotope composition does not show a bimodal composition and that quartz inclusions in the core of chloritoid have the same composition as matrix quartz demonstrates that quartz did not equilibrate its isotopic composition (Fig. 5a). This is likely due to the fact that the infiltration occurs post-deformation, and quartz

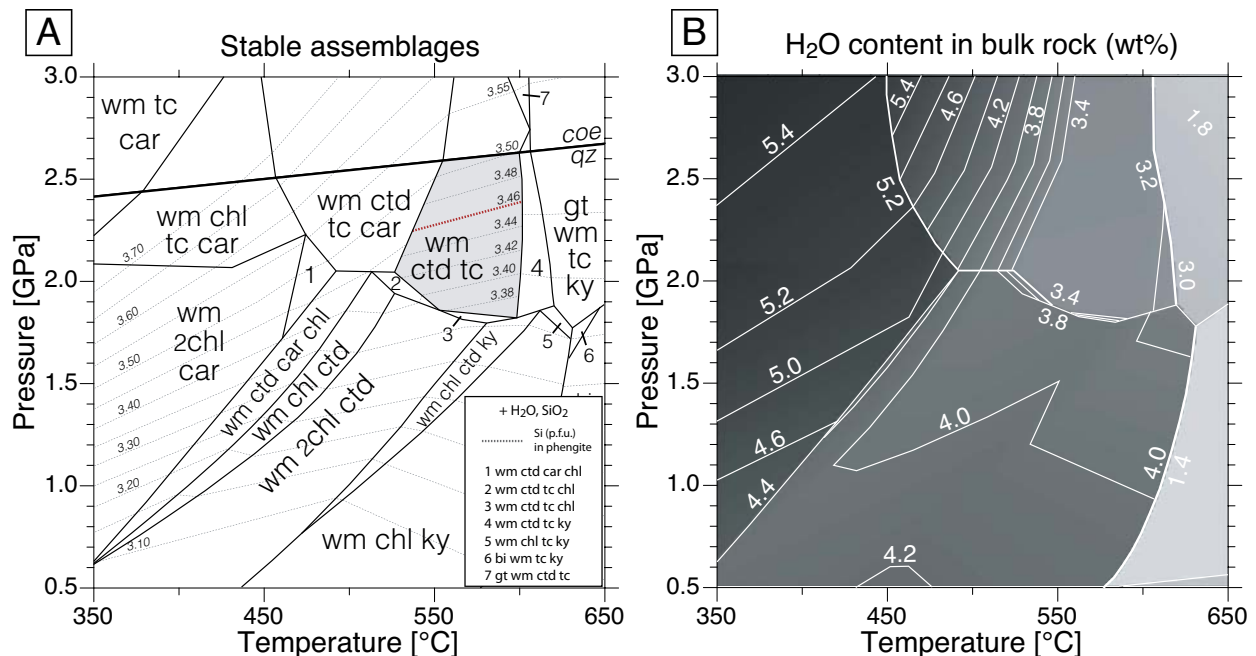


**FIGURE 8.** Thermodynamic modeling of the stable assemblages for whiteschist sample 14MR67 in the system KFMASH. The composition used is (in mole): Si(66.02), Al(18.65), Fe(1.73), Mg(9.69), K(3.91). Water saturated conditions were assumed. Quartz is present in all fields. (a) pressure ( $P$ ) and temperature ( $T$ ) diagram representing the stable assemblages. The peak pressure and temperature field is highlighted in gray and the dotted lines represent the silica content of the white mica, with the 3.46 Si apfu isopleth highlighted in bold in the peak  $P$ - $T$  field. The peak  $P$ - $T$  conditions reached during Alpine metamorphism are at a minimum 2.2 GPa and ca. 570 °C, with the corresponding mineral mode at 2.2 GPa and 570 °C: phengite: 27%, chloritoid: 18%, talc: 10%, and quartz: 45%. (b)  $P$ - $T$  diagram displaying the total  $\text{H}_2\text{O}$  content of solid phases, in wt%. The peak  $P$ - $T$  field coincides with a major dehydration reaction along the prograde evolution of the rock. (Color online.)

is not produced by the retrograde reaction, as demonstrated by the absence of quartz in the sericite rims.

The formation of retrograde white micas in the whiteschist is due to chloritoid breakdown, as shown by the microstructural record (Figs. 5a and 5c). Very fine-grained sericitic phengites replaced chloritoid. These mica crystals have Si content between 3.00 and 3.15 apfu and have  $\delta^{18}\text{O}$  values between 5.2 and 6.0‰ (Fig. 6b). The temperature of crystallization for these retrograde sericitic phengites cannot be determined directly from isotopic exchange equilibria, since no quartz in textural equilibrium could be identified. Here, we will assume that this retrograde alteration occurred during the greenschist facies event (ca. 450 °C, also suggested by Frey et al. 1976; for the retrograde metamorphic event in the Monte Rosa) or even later, at the same time as the fluids infiltrated metagranite 1, at a temperature of about 315 °C (Table 3). The pressure recorded by these sericitic phengites would be about 0.5 GPa (see Fig. 8a), assuming  $\text{H}_2\text{O}$  saturation. However, since the pseudomorphic replacement is typically arrested, leaving significant amounts of chloritoid and talc in most whiteschist samples, it seems unlikely that  $\text{H}_2\text{O}$  saturation was maintained during retrogression. Indeed, the partial replacement texture indicates that  $\text{H}_2\text{O}$  was fully consumed, suggesting  $\text{H}_2\text{O}$  fugacities significantly below  $\text{H}_2\text{O}$  saturation. Hence, this pressure should be taken with caution.

Transforming chloritoid and talc to sericitic phengite and chlorite requires fluid infiltration (see discussion above) since chlorite-phengite paragenesis contains more  $\text{H}_2\text{O}$  than chloritoid and talc assemblages (Fig. 8b). Given the abundance of phengite in the chloritoid alteration halo (Figs. 5a and 5c), this fluid also introduces potassium. The oxygen isotope composition of the fluids in equilibrium with the sericitic phengites replacing chloritoid have a calculated  $\delta^{18}\text{O}$  composition ranging between 2.5 to 6.0‰, using the fractionation factors of Zheng (1993), for a temperature range between 250 to 450 °C, respectively.

At the outcrop scale, the external rim of the whiteschist body is fully retrogressed into a greenschist-facies assemblage. The paragenesis consists of chlorite, muscovite, and quartz, and in some zones poikilitic albite. Locally, chloritoid pseudomorphs can still be identified. This means that the outer rim of the whiteschist pipe has been much more affected by retrograde fluid influx than the center of the whiteschist. This is not surprising, as lithological contacts represent favorable fluid pathways.

### Mechanism of retrograde alteration and origin of late fluids

The isotopic signatures recorded in rocks due to fluid-rock interaction can be used to understand the mechanism of alteration, and, in some cases, the origin of the fluids. Fluid-rock interaction can be classified into two end-member processes: rock-buffered or fluid-buffered (e.g., Baumgartner and Valley 2001). While fluid-buffered systems allow determination of the composition of the external fluids, this information is lost in systems that are rock dominated. Indeed, rock-buffered systems in which isotopic equilibrium is maintained for the whole rock are not interesting for isotopic studies since no changes related to fluid-rock interaction will be observed. Nevertheless, rock-buffered systems can be used very successfully if partial or local equilibrium or mass balance approaches are used (e.g., Skora et al. 2011). At any given time in the history of a fluid infiltration system, it can locally be rock-

buffered, while other parts of the system are fluid-buffered (e.g., Baumgartner and Rumble 1988; Bowman et al. 1994), especially if fluid flow is focused on heterogeneous permeability media (e.g., Baumgartner and Valley 2001; Cui et al. 2001; Gerdes et al. 1995) or by deformation (e.g., Person et al. 2007; Quilichini et al. 2015; Tartèse et al. 2012). Stable isotope compositions in the rock-dominated system, while having lost the information on the fluid source, can still be used to evaluate the reaction mechanisms in combination with phase petrology and microtexture. Below we present two end-member models based on the above discussion to interpret the retrograde alteration of the whiteschists.

**Fluid-buffered model.** The fluids infiltrating the whiteschists have low- $\delta^{18}\text{O}$  values of 2.5 to 6.0‰, assuming fluid-buffering and equilibrium of precipitated sericitic phengites at temperatures between 250 and 450 °C, respectively. Fluids with such low- $\delta^{18}\text{O}$  signatures cannot originate from the Monte Rosa metagranite or the surrounding paragneisses, since their isotopic composition is much too high, as is shown for the granite in this study (see also Darbellay 2005; Luisier et al. 2021); they have to be external to the Monte Rosa nappe. Another probable source in the geologic context of the Monte Rosa nappe is the Bündnerschiefer from the Zermatt-Saas zone (ZSZ), which can be found at a few hundred meters distance from the whiteschist outcrop discussed here (Fig. 1). Nevertheless, the Bündnerschiefer, and the mafic rocks in immediate contact with the nappe, all have higher  $\delta^{18}\text{O}$  values relative to the whiteschist (Cartwright and Barnicoat 1999; Dessimoz 2005). A more plausible source are the Zermatt-Saas serpentinites, which are abundant in the ZSZ (Steck et al. 2015). Serpentinites from the Zermatt-Saas unit have  $\delta^{18}\text{O}$  values between 0 to 5‰ in the Upper Ayas Valley (Dessimoz 2005). Fluids equilibrated or produced by these serpentinites would be a suitable source for the low  $\delta^{18}\text{O}$ , in agreement with serpentinite data from other locations in the Zermatt-Saas unit (Cartwright and Barnicoat 1999). Serpentinites can potentially release a substantial amount of fluid during dehydration reactions, as indicated by the positive slope of the antigorite breakdown reaction in a  $P$ - $T$  diagram (Kerrick and Connolly 2001; Ulmer and Trommsdorff 1995). Nevertheless, this reaction occurs at significantly higher temperatures than the proposed temperature-pressure path for the Monte Rosa nappe (Luisier et al. 2019; Vaughan-Hammon et al. 2021), so that the fluids would either have traveled a large distance through the nappe stack from hotter parts of the orogen, or that extraneous fluids (surface fluids for example) would have equilibrated with the local serpentinite stack during exhumation (e.g., Barnes et al. 2004; Philippot and Selverstone 1991). Hence, while it is not possible to exclude this model, it seems not very likely.

**Rock buffered model.** Textural observations show that the new, retrograde sericitic phengite replaces chloritoid (Figs. 3 and 5). Sericite dominates the rims and the pseudomorphs, but some chlorite is also found. An isotopic equilibrium between high-pressure phengite at peak metamorphic conditions (570 °C, 2.2 GPa; Fig. 8a) with chloritoid can be written as:

$$\delta^{18}\text{O}_{\text{ctd}} = \delta^{18}\text{O}_{\text{HPphe}} + \Delta_{\text{ctd-HPphe}}^{570^\circ\text{C}} \quad (3)$$

with  $\delta^{18}\text{O}_{\text{ctd}}$  being the  $\delta^{18}\text{O}$  of chloritoid,  $\delta^{18}\text{O}_{\text{HPphe}}$  the  $\delta^{18}\text{O}$  of the high-pressure phengite and  $\Delta_{\text{ctd-HPphe}}^{570^\circ\text{C}}$  the fractionation factor of  $\delta^{18}\text{O}$  between chloritoid and high-pressure phengite at 570 °C. The

fractionation factor used, from Zheng (1993), is  $-0.85\%$ . Hence, the oxygen isotope composition of chloritoid in equilibrium with the high-pressure phengite would be nearly  $1\%$  lighter than that of the phengite. If we assume that the amount of oxygen supplied by the fluid is negligible, e.g., assuming a rock-buffered system, then the newly crystallized phengite inherits its isotopic composition from the chloritoid; it would be roughly  $1\%$  lighter than the high-pressure sericitic phengites in the whiteschist. This agrees with the data measured: the high-pressure phengites have a composition between  $6.1$  and  $7.5\%$ , while retrograde, sericitic phengites with low-silica content have values of  $5.2$  to  $6.0\%$ .

### IMPLICATIONS

This study required the development of white mica reference materials covering the phengite solid solution for in situ oxygen isotope measurements by SIMS. Four species, among them one muscovite (UNIL\_WM1) and three phengites (UNIL\_WM2, UNIL\_WM3, and UNIL\_WM4), were found to be suitable as reference materials for SIMS analyses. They allow the measurement of the oxygen isotope composition of most white mica specimens because no compositional dependence on the celadonite content was found. The measurement repeatability is between  $0.30$  and  $0.40\%$  when using the optimal analytical conditions of  $1.5$  nA primary beam without raster. These reference materials are available upon request at the SwissSIMS facility of the University of Lausanne.

White micas crystallize over a large range of pressure and temperature conditions and are sensitive markers of fluid-rock interactions. Three Monte Rosa samples, consisting of one whiteschist and two metagranite were selected for in situ SIMS oxygen isotopes measurement of white mica and quartz to investigate fluid-rock interaction leading to metasomatism of granite, the formation of whiteschist, and their retrograde alteration. Whiteschist oxygen isotopes compositions in both white mica and quartz are significantly lower than in the metagranite and are not overlapping. Whiteschist chemistry was established before Alpine metamorphism, which resulted in the crystallization of the actual whiteschist paragenesis of talc-chloritoid-phengite-quartz. The temperature estimates for the peak metamorphic conditions with oxygen isotope fractionation between quartz and phengite ranged between  $380$  and  $540$  °C. These are lower than the  $570$  °C (at  $2.2$  GPa) obtained using thermodynamic phase petrology modeling. The large  $T$ -range observed is mostly due to the analytical uncertainty of  $\pm 0.3\%$  for quartz and  $0.3\%$  for mica. Together with the small temperature dependence of the quartz-phengite fractionation factor, this results in ca.  $60$  °C (at  $300$  °C) and  $120$  °C (at  $500$  °C) uncertainties for individual temperature estimates.

Retrograde, sericitic phengites partially replacing chloritoid crystals have lower  $\delta^{18}\text{O}$  values than the peak phengites. We suggest that only minor amounts of fluid infiltrated the whiteschists, resulting in a local rock buffering of isotopic compositions. The field and textural observations support this rock-buffered model. Sourcing the fluids from the ultramafic rocks of the Zermatt-Saas unit seems unlikely.

Larger amounts of externally derived fluids infiltrated along the granite-whiteschist contact, obliterating any chloritoid in these outer zones. In contrast, only minor retrogression is found within the whiteschist body, documenting that inside the body there was

only a very limited amount of fluid present. Hence the whiteschist-granite couple acted as a heterogeneous fluid flow system, in which fluid is concentrated at the contact, with only minor retrogression of granite and whiteschist away from the contact.

Our study allowed the distinction of several fluid events for the origin of the oxygen isotope composition of white mica and quartz in the Monte Rosa whiteschist and metagranite. A first major and pervasive event is responsible for the hydrothermal alteration of the granite into the whiteschist before the onset of Alpine orogeny, and a late, localized, fluid infiltration related to nappe exhumation was characterized. These results highlight the ability of white mica to maintain its chemical and isotopic composition throughout regional metamorphism and localized fluid-rock interactions, further demonstrating that in situ  $\delta^{18}\text{O}$  measurements in white mica are a powerful tool to monitor changes in environmental growth conditions.

### ACKNOWLEDGMENTS AND FUNDING

We thank Guillaume Siron and Florence Bégué for their help and guidance with SIMS analyses and sample preparation, Torsten Vennemann for giving us access to the stable isotope laboratory, and Martin Robyr for his assistance with EPMA data acquisition. Katharina Marger and Joshua Vaughan-Hammon and thanked for stimulating discussions. Constructive reviews by Simona Ferrando and one anonymous reviewer are gratefully acknowledged. We thank Thomas Mueller for the editorial work. This research was supported by the Swiss National Foundation grants no. 26084159 and 206021\_163991.

### REFERENCES CITED

- Bailey, S.W. (1984) Classification and structures of the micas. In S.W. Bailey, Ed., *Micas*, pp. 1–12. Reviews in Mineralogy, Mineralogical Society of America, Chantilly, Virginia.
- Barnes, J.D., Selverstone, J., and Sharp, Z.D. (2004) Interactions between serpentinite devolatilization, metasomatism and strike-slip strain localization during deep-crustal shearing in the Eastern Alps. *Journal of Metamorphic Geology*, 22, 283–300.
- Baumgartner, L.P., and Rumble, D. (1988) Transport of stable isotopes: I: Development of a kinetic continuum theory for stable isotope transport. *Contributions to Mineralogy and Petrology*, 98, 417–430.
- Baumgartner, L.P., and Valley, J.W. (2001) Stable isotope transport and contact metamorphic fluid flow. *Reviews in Mineralogy and Geochemistry*, 43, 415–467.
- Bearth, P. (1952) *Geologie und Petrographie des Monte Rosa*. Beitr. Geol. Karte Schweiz NF, 96, 94 p.
- Berman, R.G. (1988) Internally-Consistent Thermodynamic Data for Minerals in the System  $\text{Na}_2\text{O}-\text{K}_2\text{O}-\text{CaO}-\text{MgO}-\text{FeO}-\text{Fe}_2\text{O}_3-\text{Al}_2\text{O}_3-\text{SiO}_2-\text{TiO}_2-\text{H}_2\text{O}-\text{CO}_2$ . *Journal of Petrology*, 29, 445–522.
- Bowman, J.R., Willett, S.D., and Cook, S.J. (1994) Oxygen isotopic transport and exchange during fluid flow: One-dimensional models and applications. *American Journal of Science*, 294, 1–55.
- Bucher, K., and Grapes, R. (2011) *Metamorphism of Mafic Rocks*. In K. Bucher and R. Grapes, Eds., *Petrogenesis of Metamorphic Rocks*, p. 339–393. Springer.
- Bucher-Nurminen, K., Frank, E., and Frey, M. (1983) A model for the progressive regional metamorphism of margarite-bearing rocks in the Central Alps. *American Journal of Science* 283-A, 370–395.
- Bulle, F., Rubatto, D., Ruggieri, G., Luisier, C., Villa, I.M., and Baumgartner, L. (2020) Episodic hydrothermal alteration recorded by microscale oxygen isotope analysis of white mica in the Larderello-Travale Geothermal Field, Italy. *Chemical Geology*, 532, 119288.
- Cartwright, I., and Barnicoat, A.C. (1999) Stable isotope geochemistry of Alpine ophiolites: a window to ocean-floor hydrothermal alteration and constraints on fluid-rock interaction during high-pressure metamorphism. *International Journal of Earth Sciences*, 88, 219–235.
- Chopin, C. (1985) Les relations de phase dans les métapelites de haute pression. Approche expérimentale et naturaliste, conséquences géodynamiques pour les Alpes occidentales, Paris. University Pierre et Marie Curie—Paris VI.
- Chopin, C., and Monié, P. (1984) A unique magnesiochloritoid-bearing, high-pressure assemblage from the Monte Rosa, Western Alps: Petrologic and  $40\text{Ar}-39\text{Ar}$  radiometric study. *Contributions to Mineralogy and Petrology*, 87, 388–398.
- Coplen, T.B., Kendall, C., and Hopple, J. (1983) Comparison of stable isotope reference samples. *Nature*, 302, 236–238.
- Cui, X., Nabelek, P.L., and Liu, M. (2001) Heat and fluid flow in contact metamorphic aureoles with layered and transient permeability, with application to the Notch Peak aureole, Utah. *Journal of Geophysical Research: Solid Earth*, 106, 6477–6491.
- Dal Piaz, G.V. (2001) *Geology of the Monte Rosa massif: historical review and personal*

- comments. *Schweizerische Mineralogische Und Petrographische Mitteilungen*, 81, 275–303.
- Darbellay, B. (2005) Histoire polymétamorphique de la nappe du Mont Rose et contraintes isotopiques. Master Thesis. University of Lausanne, Switzerland.
- de Capitani, C., and Brown, T.H. (1987) The computation of chemical equilibrium in complex systems containing non-ideal solutions. *Geochimica et Cosmochimica Acta*, 51, 2639–2652.
- Dessimo, M. (2005) Métamorphisme et déformation entre la zone de Zermatt-Saas et la zone du Combin, Val d'Ayas, Italie. Master Thesis. University of Lausanne, Switzerland.
- Eiler, J.M., Graham, C., and Valley, J.W. (1997) SIMS analysis of oxygen isotopes: matrix effects in complex minerals and glasses. *Chemical Geology*, 138, 221–244.
- Eiler, J.M., Valley, J.W., and Baumgartner, L.P. (1993) A new look at stable isotope thermometry. *Geochimica et Cosmochimica Acta*, 57, 2571–2583.
- Eslinger, E.V., Savin, S.M., and Yeh, H.-W. (1979) Oxygen isotope geothermometry of diagenetically altered shales. *SEPM Special Publication*, 26, 113–124.
- Ferrando, S. (2012) Mg-metasomatism of metagranitoids from the Alps: genesis and possible tectonic scenarios. *Terra Nova*, 24, 423–436.
- Frey, M., Hunziker, J.C., O'Neil, J.R., and Schwander, H.W. (1976) Equilibrium-dis-equilibrium relations in the Monte Rosa Granite, Western Alps: Petrological, Rb-Sr and stable isotope data. *Contributions to Mineralogy and Petrology*, 55, 147–179.
- Gardien, V., Thompson, A.B., and Ulmer, P. (2000) Melting of biotite + plagioclase + quartz gneisses: The role of H<sub>2</sub>O in the stability of amphibole. *Journal of Petrology*, 41, 651–666.
- Gerdes, M.L., Baumgartner, L.P., and Person, M. (1995) Stochastic permeability models of fluid flow during contact metamorphism. *Geology*, 23, 945–948.
- Guidotti, C.V., and Sassi, F.P. (1998) Petrogenetic significance of Na-K white mica mineralogy: Recent advances for metamorphic rocks. *European Journal of Mineralogy*, 10, 815–854.
- Kerrick, D.M., and Connolly, J.A.D. (2001) Metamorphic devolatilization of subducted marine sediments and the transport of volatiles into the Earth's mantle. *Nature*, 411, 293–296.
- Kita, N.T., Huberty, J.M., Kozdon, R., Beard, B.L., and Valley, J.W. (2011) High-precision SIMS oxygen, sulfur and iron stable isotope analyses of geological materials: accuracy, surface topography and crystal orientation. *Surface and Interface Analysis*, 43, 427–431.
- Lacroix, B., and Vennemann, T. (2015) Empirical calibration of the oxygen isotope fractionation between quartz and Fe-Mg chlorite. *Geochimica et Cosmochimica Acta*, 149, 21–31.
- Lapen, T.J., Johnson, C.M., Baumgartner, L.P., Piaz, G.V.D., Skora, S., and Beard, B.L. (2006) Coupling of oceanic and continental crust during Eocene eclogite-facies metamorphism: evidence from the Monte Rosa nappe, western Alps. *Contributions to Mineralogy and Petrology*, 153, 139–157.
- Le Bayon, R., Capitani, C. D., and Frey, M. (2006) Modelling phase-assemblage diagrams for magnesian metapelites in the system K<sub>2</sub>O-FeO-MgO-Al<sub>2</sub>O<sub>3</sub>-SiO<sub>2</sub>-H<sub>2</sub>O: Geodynamic consequences for the Monte Rosa nappe, Western Alps. *Contributions to Mineralogy and Petrology*, 151, 395–412.
- Luisier, C., Baumgartner, L., Schmalholz, S.M., Siron, G., and Vennemann, T. (2019) Metamorphic pressure variation in a coherent Alpine nappe challenges lithostatic pressure paradigm. *Nature Communications*, 10, 4734.
- Luisier, C., Baumgartner, L.P., Putlitz, B., and Vennemann, T. (2021) Whiteschist genesis through metasomatism and metamorphism in the Monte Rosa nappe (Western Alps). *Contributions to Mineralogy and Petrology*, 176, 10.
- Marger, K., Luisier, C., Baumgartner, L.P., Putlitz, B., Dutrow, B.L., Bouvier, A.-S., and Dini, A. (2019) Origin of Monte Rosa whiteschist from in-situ tourmaline and quartz oxygen isotope analysis by SIMS using new tourmaline reference materials. *American Mineralogist*, 104, 1503–1520.
- Massonne, H.-J., and Schreyer, W. (1987) Phengite geobarometry based on the limiting assemblage with K-feldspar, phlogopite, and quartz. *Contributions to Mineralogy and Petrology*, 96, 212–224.
- Massonne, H.-J., and Szpurka, Z. (1997) Thermodynamic properties of white micas on the basis of high-pressure experiments in the systems K<sub>2</sub>O-MgO-Al<sub>2</sub>O<sub>3</sub>-SiO<sub>2</sub>-H<sub>2</sub>O and K<sub>2</sub>O-FeO-Al<sub>2</sub>O<sub>3</sub>-SiO<sub>2</sub>-H<sub>2</sub>O. *Lithos*, 41, 229–250.
- O'Neil, J.R., Shaw, S.E., and Flood, R.H. (1977) Oxygen and hydrogen isotope compositions as indicators of granite genesis in the New England Batholith, Australia. *Contributions to Mineralogy and Petrology*, 62, 313–328.
- Pattison, D.R.M., and Harte, B. (1991) Petrography and Mineral Chemistry of Pelites. In G. Voll, J. Töpel, D.R.M. Pattison, and F. Seifert, Eds., *Equilibrium and Kinetics in Contact Metamorphism: The Ballachulish Igneous Complex and Its Aureole*, p. 135–179. Springer.
- Pawlig, S. (2001) Geological evolution of the Monte Rosa: Constraints from geochronology and geochemistry of a talc-kyanite-chloritoid shear zone within the Monte Rosa Granite (Monte Rosa Nappe, Italian Western Alps), Ph.D. thesis, 149 p. University of Mainz, Germany.
- Pawlig, S., and Baumgartner, L.P. (2001) Geochemistry of a talc-kyanite-chloritoid shear zone within the Monte Rosa granite, Val d'Ayas, Italy. *Schweizerische Mineralogische Und Petrographische Mitteilungen*, 81, 329–346.
- Person, M., Mulch, A., Teyssier, C., and Gao, Y. (2007) Isotope transport and exchange within metamorphic core complexes. *American Journal of Science*, 307, 555–589.
- Philippot, P., and Selverstone, J. (1991) Trace-element-rich brines in eclogitic veins: implications for fluid composition and transport during subduction. *Contributions to Mineralogy and Petrology*, 106, 417–430.
- Quilichini, A., Siebenaller, L., Nachlas, W.O., Teyssier, C., Vennemann, T.W., Heizler, M.T., and Mulch, A. (2015) Infiltration of meteoric fluids in an extensional detachment shear zone (Kettle dome, WA, U.S.A.): How quartz dynamic recrystallization relates to fluid-rock interaction. *Journal of Structural Geology*, 71, 71–85.
- Rieder, M., Cavazzini, G., D'yakonov, Y.S., Frank-Kamenetskii, V.A., Gottardi, G., Guggenheim, S., Koval', P.V., Müller, G., Neiva, A.M.R., Radoslovich, E.W., and others (1999) Nomenclature of the micas. *Mineralogical Magazine*, 63, 267–279.
- Schreyer, P.D.W. (1974) Whiteschist, a new type of metamorphic rock formed at high pressures. *Geologische Rundschau*, 63, 597–609.
- Schreyer, W. (1973) Whiteschist: A high-pressure rock and its geologic significance. *The Journal of Geology*, 81, 735–739.
- Seitz, S., Baumgartner, L.P., Bouvier, A.-S., Putlitz, B., and Vennemann, T. (2017) Quartz reference materials for oxygen isotope analysis by SIMS. *Geostandards and Geoanalytical Research*, 41, 69–75.
- Sharp, Z.D., Essene, E.J., and Hunziker, J.C. (1993) Stable isotope geochemistry and phase equilibria of coesite-bearing whiteschists, Dora Maira Massif, western Alps. *Contributions to Mineralogy and Petrology*, 114, 1–12.
- Siron, G., Baumgartner, L., Bouvier, A.-S., Putlitz, B., and Vennemann, T. (2017) Biotite reference materials for secondary ion mass spectrometry <sup>18</sup>O/<sup>16</sup>O measurements. *Geostandards and Geoanalytical Research*, 41, 243–253.
- Skora, S., Baumgartner, L.P., and Vennemann, T.W. (2011) Modelling changes in stable isotope compositions of minerals during net transfer reactions in a contact aureole: Wollastonite growth at the northern Hunter Mountain Batholith (Death Valley National Park, U.S.A.). *Chemical Geology*, 289, 197–209.
- Skora, S., and Blundy, J. (2010) High-pressure hydrous phase relations of radiolarian clay and implications for the involvement of subducted sediment in arc magmatism. *Journal of Petrology*, 51, 2211–2243.
- Skora, S., Mahlen, N.J., Johnson, C.M., Baumgartner, L.P., Lapen, T.J., Beard, B.L., and Szilvagi, E.T. (2015) Evidence for protracted prograde metamorphism followed by rapid exhumation of the Zermatt-Saas Fee ophiolite. *Journal of Metamorphic Geology*, 33, 711–734.
- Spear, F.S. (1995) *Metamorphic Phase Equilibria and Pressure-Temperature-Time Paths*, 799 p. Mineralogical Society of America.
- Steck, A., Masson, H., and Robyr, M. (2015) Tectonics of the Monte Rosa and surrounding nappes (Switzerland and Italy): Tertiary phases of subduction, thrusting and folding in the Pennine Alps. *Swiss Journal of Geosciences*, 108, 3–34.
- Tartèse, R., Boulvais, P., Poujol, M., Chevalier, T., Paquette, J.-L., Ireland, T.R., and Delouie, E. (2012) Mylonites of the South Armorican Shear Zone: Insights for crustal-scale fluid flow and water-rock interaction processes. *Journal of Geodynamics*, 56–57, 86–107.
- Ulmer, P., and Trommsdorff, V. (1995) Serpentine stability to mantle depths and subduction-related magmatism. *Science*, 268, 858–861.
- Valley, J.W., and Kita, N.T. (2009) In situ oxygen isotope geochemistry by ion microprobe. MAC Short Course: Secondary Ion Mass Spectrometry in the Earth Sciences, 41, 19–63.
- Vaughan-Hammon, J.D., Luisier, C., Baumgartner, L.P., and Schmalholz, S.M. (2021) Peak Alpine metamorphic conditions from staurolite-bearing metapelites in the Monte Rosa nappe (Central European Alps) and geodynamic implications. *Journal of Metamorphic Geology*, 39, 897–917. n.d. <https://doi.org/10.1111/jmg.12595>.
- Zheng, Y.-F. (1993) Calculation of oxygen isotope fractionation in hydroxyl-bearing silicates. *Earth and Planetary Science Letters*, 120, 247–263.

MANUSCRIPT RECEIVED MARCH 26, 2020

MANUSCRIPT ACCEPTED APRIL 15, 2021

MANUSCRIPT HANDLED BY THOMAS MUELLER

### Endnote:

<sup>1</sup>Deposit item AM-22-57523, Online Materials. Deposit items are free to all readers and found on the MSA website, via the specific issue's Table of Contents (go to [http://www.minsocam.org/MSA/AmMin/TOC/2022/May2022\\_data/May2022\\_data.html](http://www.minsocam.org/MSA/AmMin/TOC/2022/May2022_data/May2022_data.html)).

### NOTE ADDED IN PROOF

The authors acknowledge the following paper published while this article was in press.

Vaughan-Hammon, J.D., Luisier, C., Baumgartner, L.P., and Schmalholz, S.M. (2021) Alpine peak pressure and tectono-metamorphic history of the Monte Rosa nappe: evidence from the cirque du Vêraz, upper Ayas valley, Italy. *Swiss Journal of Geosciences*, 114, 1, 20. <https://doi.org/10.1186/s00015-021-00397-3>